A&A 562, A89 (2014)
DOI: 10.1051/0004-6361/201322797

Astronomy & Astrophysics

The post-common-envelope, binary central star of the planetary nebula Hen 2-11⋆

D. Jones[1,2], H. M. J. Boffin[1], B. Miszalski[3,4], R. Wesson[1], R. L. M. Corradi[5,6], and A. A. Tyndall[1,7]

[1] European Southern Observatory, Alonso de Córdova 3107, 19001 Casilla, Santiago, Chile
e-mail: [djones;hboffin]@eso.org
[2] Universidad de Atacama, Copayapu 485, Copiapó, Chile
[3] South African Astronomical Observatory, PO Box 9, Observatory, 7935 Cape Town, South Africa
[4] Southern African Large Telescope Foundation, PO Box 9, Observatory, 7935 Cape Town, South Africa
[5] Instituto de Astrofísica de Canarias, 38200 La Laguna, Tenerife, Spain
[6] Departamento de Astrofísica, Universidad de La Laguna, 38206 La Laguna, Tenerife, Spain
[7] Jodrell Bank Centre for Astrophysics, School of Physics and Astronomy, University of Manchester, Manchester M13 9PL, UK

Received 4 October 2013 / Accepted 2 January 2014

ABSTRACT

We present a detailed photometric study of the central star system of the planetary nebula Hen 2-11, selected for study because of its low-ionisation filaments and bipolar morphology – traits which have been strongly linked with central star binarity. Photometric monitoring with NTT-EFOSC2 reveals a highly irradiated, double-eclipsing, post-common-envelope system with a period of 0.609 d. Modelling of the lightcurve indicates that the nebular progenitor is extremely hot, while the secondary in the system is probably a K-type main sequence star. The chemical composition of the nebula is analysed, showing Hen 2-11 to be a medium-excitation non-Type I nebula. A simple photoionisation model is constructed determining abundance ratios of C/O and N/O which would be consistent with the common-envelope cutting short the AGB evolution of the nebular progenitor. The detection of a post-common-envelope binary system at the heart of Hen 2-11 further strengthens the link between binary progeny and the formation of axisymmetric planetary nebulae with patterns of low-ionisation filaments, clearly demonstrating their use as morphological indicators of central star binarity.

Key words. binaries: close – binaries: eclipsing – circumstellar matter – ISM: abundances – stars: AGB and post-AGB – planetary nebulae: individual: Hen 2-11

1. Introduction

It is now clear that common-envelope (CE) evolution represents an important channel for the formation of planetary nebulae (PNe), constituting a significant fraction of the total PN population (Miszalski et al. 2009a). However, in-depth analysis of this population, as well as their influence on the host nebulae, is still hampered by the small sample and lack of detailed study for individual objects. It is, therefore, critical to the field that further binary central stars are discovered and characterised.

Recent work has shown that PNe with post-CE, binary central stars show a penchant for low-ionisation filaments and axisymmetrical structures (Miszalski et al. 2009b, 2011b), as such PNe displaying these traits should offer the greatest chance of binary discovery. While spectroscopic monitoring for radial velocity variables has shown promising results (e.g. Boffin et al. 2012b), the most efficient methodology remains photometric monitoring (Miszalski et al. 2009a, 2011a).

Hen 2-11 (PN G259.1+00.9; $\alpha = 08^{h}37^{m}08.3^{s}$, $\delta = -39°25'08''$) is a southern PN first detected by Henize (1967). The nebula was shown by Górny et al. (1999) to display an elongated morphology with low-ionisation filaments. Based on its similar appearance in this image to two other post-CE PNe, NGC 6326 and NGC 6778 (Miszalski et al. 2011b), we selected it as a promising candidate for photometric monitoring as part of ongoing efforts by our team to discover binary central stars (Corradi et al. 2011; Miszalski et al. 2011a,b, 2013b; Tyndall et al. 2013). Here, we report on the discovery of an eclipsing post-CE central star displaying a strong irradiation effect that is reminiscent of Abell 63 (Pollacco & Bell 1993) and Abell 46 (Pollacco & Bell 1994). The discovery of rare eclipsing central stars is a key step towards measuring accurate, model-independent central star masses for a large sample of PNe (Miszalski et al. 2008).

The paper is structured as follows. Section 2 outlines the observations and data reduction, Sect. 3 describes the light curve analysis and modelling, and the analysis of the stellar and nebular spectroscopy. Finally, Sect. 4 discusses the results.

2. Observations and data reduction

2.1. Photometry

The central star of Hen 2-11 was monitored photometrically with EFOSC2 on the 3.6-m ESO-NTT (Buzzoni et al. 1984; Snodgrass et al. 2008) on the nights of 27–29 February, 1–2 March 2012, and 14, 15 and 17 January 2013. The observations employed the *i#705* (Gunn *i*) filter and E2V CCD with a pixel scale of 0.24″ × 0.24″ pixel^{-1}. A total of 200 *I*-band observations were taken with 60-s exposure

⋆ Extracted 1D spectra, reduced 2D spectra, and table of photometry are only available at the CDS via anonymous ftp to cdsarc.u-strasbg.fr (130.79.128.5) or via http://cdsarc.u-strasbg.fr/viz-bin/qcat?J/A+A/562/A89

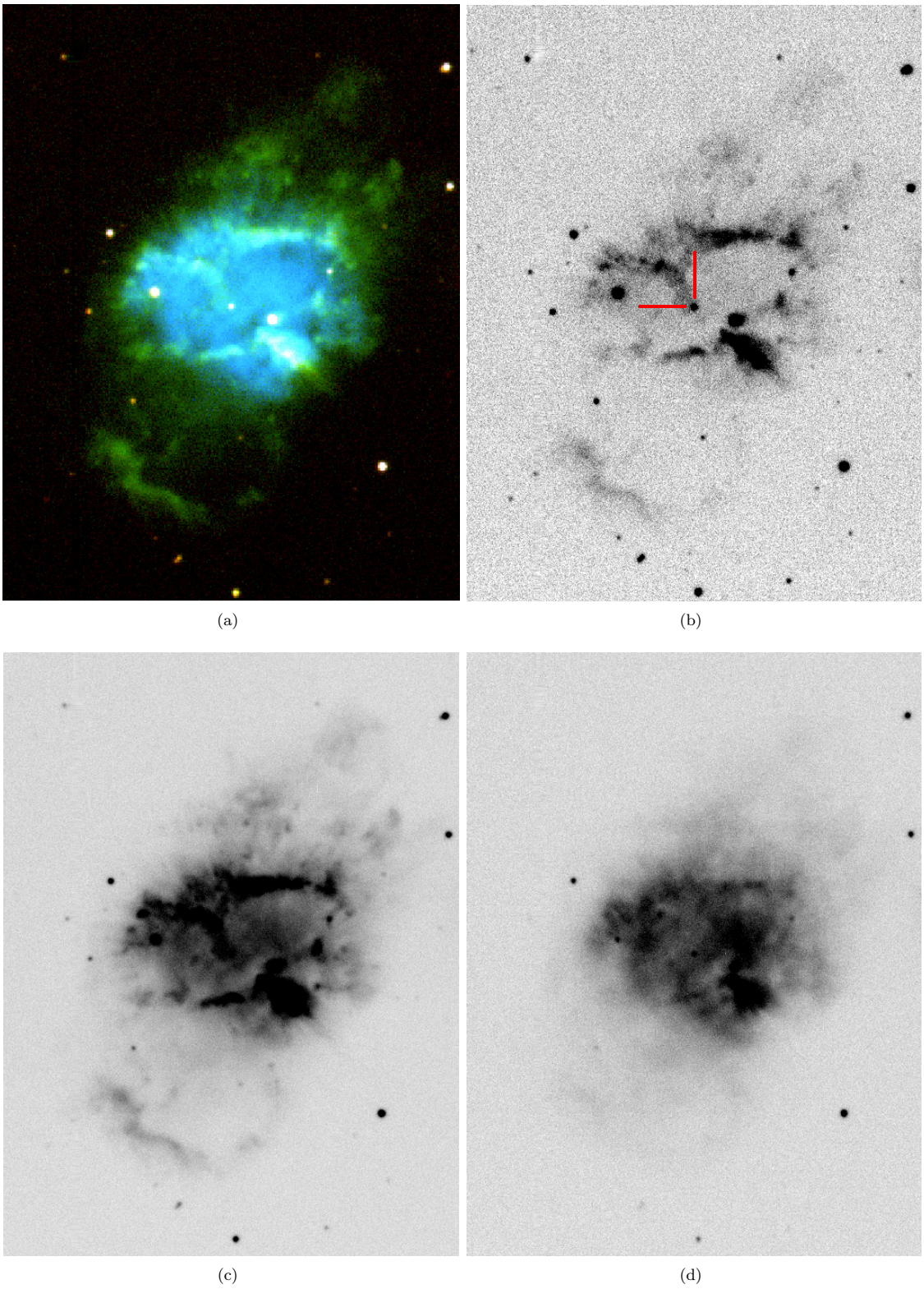

Fig. 1. NTT-EFOSC2 images of Hen 2-11. **a)** Colour composite made from [S II] λ6716+6731 Å (red), Hα+[N II] (green) and [O III] λ5007 Å (blue), **b)** [S II] λ6716+6731 Å with the central star marked, **c)** Hα+[N II] and **d)** [O III] λ5007 Å. North is up, east to the left and each image measures $2' \times 3'$.

time. Further individual observations of 240-s were acquired with narrowband [O III] λ5007 Å (*#687*), Hα+[N II] (*#692*) and [S II] λ6716+6731 Å (*#700*) filters, two exposures of 20 s with a Bessel *B* filter (*#639*) and five of 180-s in Hβ-continuum (*#743*). A three-colour composite image of the nebula is presented in Fig. 1, along with the individual images taken in the narrowband emission line filters.

All data were debiased and flat-fielded using standard STARLINK routines[1]. Photometry was extracted using SEXTRACTOR

[1] http://starlink.jach.hawaii.edu/

Table 1. Log of the SALT RSS observations.

Date (DD/MM/YY)	JD	ϕ	Grating	Exptime (s)	λ ($''$)	$\Delta\lambda$ (*FWHM*, Å)	Dispersion (Å pix^{-1})
22/12/12	2 456 282.412835	0.93	PG900	2350	3907–7004	6.0	0.98
21/03/13	2 456 373.421354	0.30	PG900	2350	6300–9290	5.5	0.95
13/04/13	2 456 396.353935	0.94	PG1300	2500	4082–6178	4.3	0.66

Notes. The slit-width for all observations was 1.50 Å.

with an aperture tailored to a diameter of 3× the seeing on each frame (Bertin & Arnouts 1996; Jones 2011), and the differential *I*-band mag of the central star measured against non-variable field stars. An absolute scale, with an approximate precision of 0.05 mag (derived from the dispersion in detector zero points calculated for each field star), was applied to the data via the methodology described in Boffin et al. (2012a) using catalogue photometry from DENIS (Epchtein et al. 1999).

2.2. Spectroscopy

Table 1 outlines the spectroscopic observations of Hen 2-11 made with the Robert Stobie Spectrograph (RSS; Burgh et al. 2003; Kobulnicky et al. 2003) of the Southern African Large Telescope (SALT; Buckley et al. 2006; O'Donoghue et al. 2006). The position angle (PA) of the slit was selected to be 71.5°, to include the brighter star to the southwest of the central star. Basic reductions were applied using the PySALT[2] package (Crawford et al. 2010). Contemporaneous spectroscopic flat-fields were taken with each PG900 spectrum and were applied to the science exposures after each flat was divided by a 50 pixel median of itself to reduce the amplitude of fringing on the detectors and to correct bad pixels. Cosmic ray events were cleaned using the LACOSMIC package (van Dokkum 2001). Wavelength calibration of arc lamp exposures was performed using standard IRAF[3] tasks IDENTIFY, REIDENTIFY, FITCOORDS and TRANSFORM by identfying the arc lines in each row and applying a geometric transformation to the data frames. One dimensional spectra were extracted for the central star and the nebula, keeping the same aperture in the separate exposures. Spectrophotometric standard stars were used to flux calibrate the spectra in the usual fashion. Due to the moving pupil design of SALT only a relative (not absolute) spectrophotometric solution can be obtained.

3. Analysis

3.1. Morphology

The narrowband images presented in Fig. 1 show Hen 2-11 to comprise a bright central region roughly 1′ in diameter with an irregular patten of low-ionisation filamentary structures extending out to the northwest and southeast. As commented on in Sect. 1, the nebula bears a striking resemblance to two other PNe previously shown to host binary nuclei, NGC 6326 and NGC 6778 (Miszalski et al. 2011b). The central region of the nebula is bright and relatively uniform in [O III] λ5007 Å (Fig. 1d), while in the light of [S II] λ6716+6731 Å and Hα+[N II] the central structure appears far more filamentary (low-ionisation filaments like these are found in both NGC 6326 and NGC 6778; Miszalski et al. 2011b). Away from the central region, there is little emission in [O III] λ5007 Å, but the [S II] λ6716+6731 Å and Hα+[N II] images reveal bipolar extensions up to 80″ from the central star to both the northwest and southeast. A particularly bright filament is found at the tip of the southeastern lobe, running perpendicular to the major axis of the nebula, while the northwestern projection has a more floccular appearance. These structures may perhaps be high velocity outflows/jets similar to those seen in NGC 6778 (Guerrero & Miranda 2012), features which are hypothesised to be formed by mass transfer in a binary system (Miszalski et al. 2013a; Tocknell et al. 2013).

3.2. Lightcurve

A Lomb-Scargle analysis was performed in order to determine the periodicity of the variability displayed by the central star of Hen 2-11 using the PERIOD package of the STARLINK software suite (Dhillon et al. 2001). Figure 2 shows the data folded on the ephemeris determined by the analysis,

$$\min I = 2\,455\,988.1617(\pm0.0005) + 0.6093(\pm0.0003)\mathrm{E}. \quad (1)$$

The lightcurve shows smooth sinusoidal variation of peak-to-peak amplitude ∼1.1 mag, with eclipses at phases 0 and 0.5. The primary eclipse, at phase 0, is approximately 1.5 mag deep, indicating that even in the *I*-band much of the flux originates from the hot nebular progenitor. As such, the sinusoidal variability can be attributed to the primary irradiating the near face of the secondary, and the changing projection of this face with the binary orbit (often referred to as a reflection or irradiation effect). The strength of this reflection effect, as well as the pronounced secondary eclipse, indicate that the inclination of the system must also be close to 90°.

The system was modelled using the NIGHTFALL code[4]. All parameters were varied over a wide range of physical solutions, with the final model being selected for having the lowest χ^2 fit. A "third light" component (of 9.5% at mean mag in the *I*-band) was incorporated into the model. This value is based on an estimation of the remaining nebular contamination following the background fitting and subtraction performed by SEXTRACTOR. The estimation was carried out by measuring the flux, on a selection of background subtracted images produced by SEXTRACTOR, in an annulus surrounding the central star and comparing that to the flux in an aperture centred on the sky background away from the nebula, and then scaling this flux to that which would contaminate an aperture of radius 1.5× the median seeing of the observations. Given the obviously large reflection effect in the system, detailed reflection was employed in the modelling

[2] http://pysalt.salt.ac.za

[3] IRAF is distributed by the National Optical Astronomy Observatory, which is operated by the Association of Universities for Research in Astronomy (AURA) under cooperative agreement with the National Science Foundation.

[4] http://www.hs.uni-hamburg.de/DE/Ins/Per/Wichmann/Nightfall.html

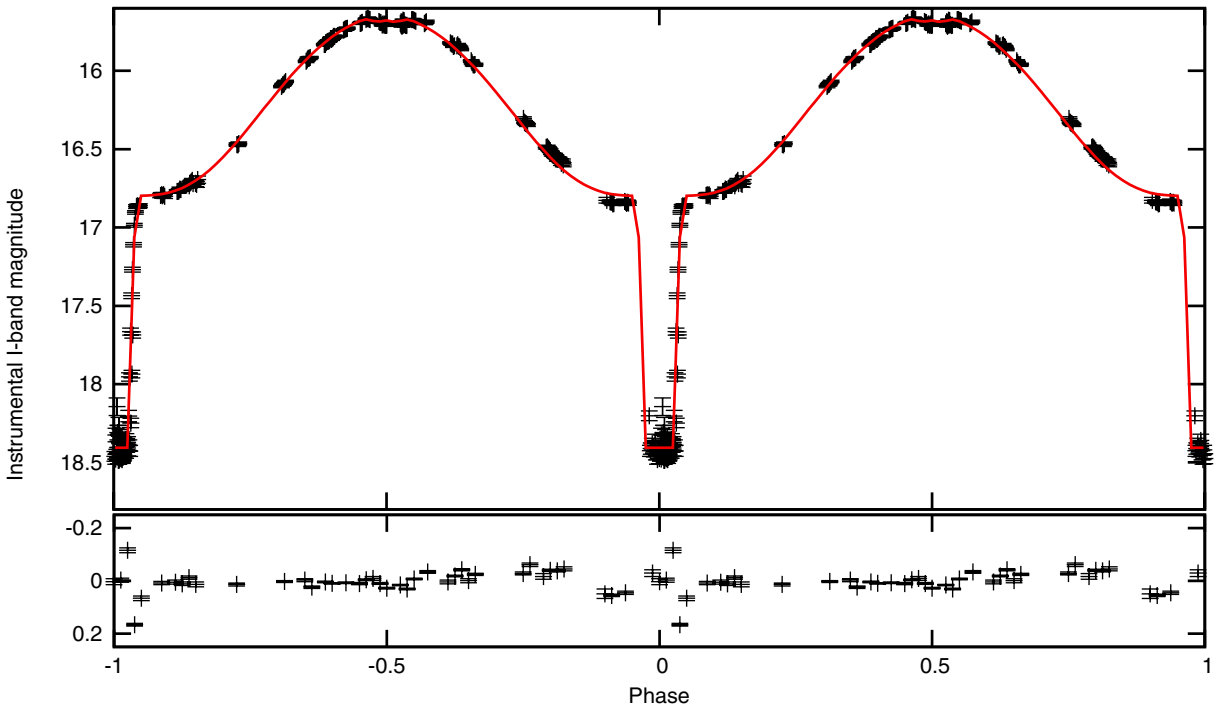

Fig. 2. Folded NTT-EFOSC2 *I*-band photometry of the central star of Hen 2-11 with the NIGHTFALL model overlaid in red (*upper panel*). Binned residuals between the observed photometry and model are shown in the *lower panel*. Note that the size of the points represents the photometric uncertainty and contain no estimate of the uncertainty due to variable nebular contamination (which can be significant, see text for details).

Table 2. Modelled and observed binary parameters.

	Primary	Secondary
$T_{\rm eff}$ (K)	$140\,000 \pm 30\,000$	4500 ± 500
Radius ($R_\odot$)	0.13 ± 0.02	0.68 ± 0.03
Log g	–	4.5[a]
Inclination	$90° \pm 0.5°$	
M_1/M_2	$0.91^{+0.11}_{-0.14}$	
Period (d)	0.6093 ± 0.0003	
Peak-to-peak I-mag amplitude of irradiation effect	1.12 ± 0.07	
Min. I-mag of sinusoidal region of lightcurve	16.80 ± 0.05[b]	
Eclipse I-mag	18.40 ± 0.05[c]	
Extinction-corrected min. V-mag of sinusoidal region	13.82 ± 0.08[d]	
Extinction-corrected eclipse V-mag	17.36 ± 0.08[e]	

Notes. [(a)] A fixed parameter in the modelling. [(b)] Measured value, not accounting for nebular contamination of roughly 10% at this phase. [(c)] Measured value, not accounting for nebular contamination of roughly 25% at this phase. [(d)] Corrected using the measured $c(\mathrm{H}\beta) = 2.42 \pm 0.04$, and a representative $(V-I)_0 = -0.4$ for the nebular progenitor (Ciardullo et al. 1999). [(e)] Corrected using the measured $c(\mathrm{H}\beta) = 2.42 \pm 0.04$, and assuming that the modelled temperature is representative of the spectral type of the secondary (see text for details).

(with 5 iterations) in order to properly treat the irradiation of the secondary by the primary. A model atmosphere was used for the lower temperature (secondary) component with solar metallicity and log g of 4.5 (Kurucz 1993). The final model lightcurve is shown, along with the residuals to the binned data, in Fig. 2 and the model parameters outlined in Table 2.

In general, the model fits well, with residuals of less than 0.05 mag at most phases (reasonable considering the errors plotted are solely from the photometry and do not account for the variable nebular contamination). The worst fit is attained around primary eclipse, where the percentage contribution from the nebula is at a maximum and the data is of lowest signal-to-noise, due to the intrinsic faintness of the secondary. The additional scatter in the data around this phase could also be due to star spots, however this is impossible to ascertain given the signal-to-noise and time coverage of our data. In order to fully assess the validity of the model, it is important to compare the model parameters to the observations (as well as theory, where possible) and ensure the two are consistent.

The model parameters (namely temperature and radius) for the secondary indicate that it has an absolute bolometric magnitude, $M_{\rm bol}$, equal to 6.7 and is roughly of spectral type K5V (Boyajian et al. 2012). Adopting a bolometric correction of −0.66 (Kaler 1989), a $(V-I)_0$ colour of 1.54 (Ducati et al. 2001) and an extinction, $c(\mathrm{H}\beta)$, of 2.41 (determined from our SALT spectroscopy, see Sect. 3.3), and using the reddening law of Howarth (1983), we calculate the distance to be roughly 700 pc (assuming the I-mag at eclipse is that of the secondary

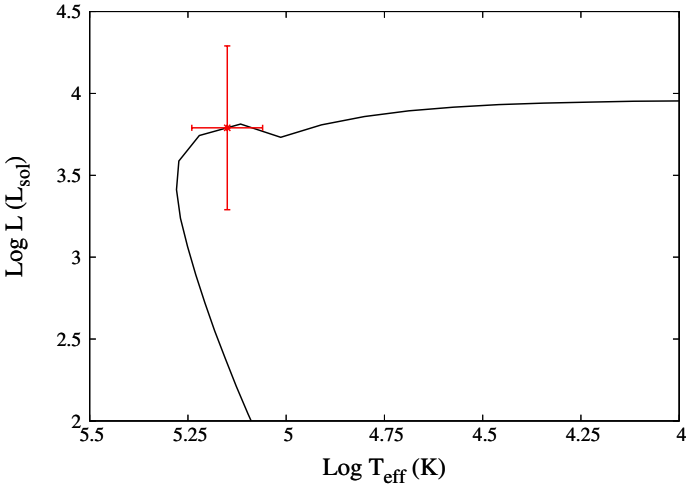

Fig. 3. Helium-burning evolutionary track for M_i = 2.5 $M_\odot$, M_f = 0.67 $M_\odot$ from Vassiliadis & Wood (1994), with the location of the model central star of Hen 2-11 marked (corresponding to an age of approximately 7000 years).

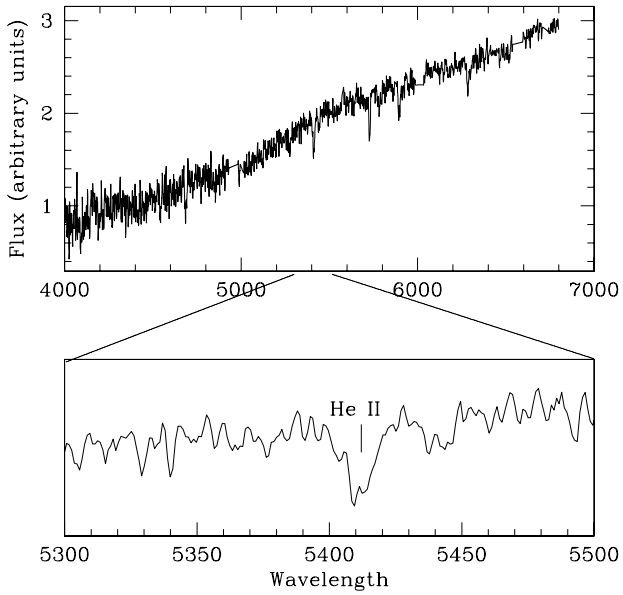

Fig. 4. Low-resolution SALT spectrum of the central star of Hen 2-11 taken at a phase of ϕ = 0.93. The *zoom* displays the region around the He II λ5412 Å absorption feature.

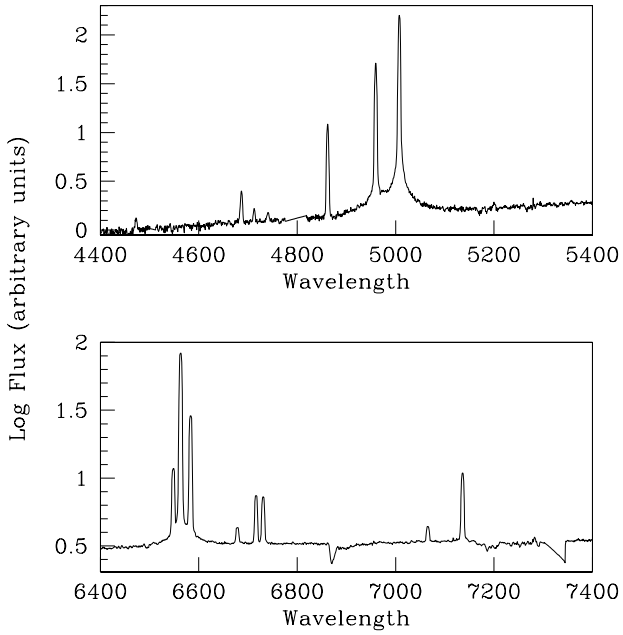

Fig. 5. A combined nebular spectrum of Hen 2-11, composited from the three exposures listed in Table 1.

and accounting for the nebular contamination at this phase of ~0.3 mag). While this distance is a little on the low side, it is still within the error margins of the statistical distance calculated by Stanghellini et al. (2008, of 890 pc) and the distance by trigonometric parallax of ~780 pc (Gutiérrez-Moreno et al. 1999). We recalculated the distance using the Stanghellini et al. (2008) method, our extinction value, a radius of 32″ and log $F(\mathrm{H}\beta)$ = −12.14 (Acker et al. 1992). This yields 817 pc, more in line with the proper-motion based distance and offering a better agreement with our distance.

The spectral type of the secondary and the modelled mass ratio imply a mass for the primary of roughly 0.67 $M_\odot$. However, determinations of spectral type based solely on modelling of the lightcurve are notoriously unreliable in these systems (see Sect. 4). It is interesting to note that in spite of the significant uncertainties, the modelled effective temperature and luminosity lie on the evolutionary track for a 0.67 $M_\odot$ remnant (formed from a 2.5 $M_\odot$ progenitor) with an age of ~7000 years (Fig. 3). This is a reasonable age for a planetary nebula, and would imply an expansion velocity, $v_{\rm exp}$, of roughly 30–40 km s^{-1} (given the distance to and angular size of the observed nebula), which is fairly typical for a PN with a binary central star (e.g. Jones et al. 2010, though greater than the average for PNe in general). Collectively, this shows that our model provides a reasonable solution to the systemic parameters, in spite of the lack of radial velocity study which would be required in order to provide stronger constraints (see Sect. 4).

3.3. Stellar and nebular spectra

Figure 4 shows the low-resolution PG900 spectrum of the central star with weak absorption from He II λ5412 Å detected on top of a heavily reddened continuum, confirming it to be the ionising source of the PN. The lack of emission lines is consistent with the irradiated zone of the secondary facing away from us at the phase observed.

The extracted nebular spectra were combined to produce a single spectrum with wavelength coverage from ~4000–9000 Å (shown in Fig. 5). From the ratios of Hα, Hγ and Hδ to Hβ, and using the Galactic extinction law of Howarth (1983), we determine the logarithmic extinction at Hβ, c(Hβ), to be 2.41 ± 0.01. This is almost 0.2 dex greater than that found by Shaw & Kaler (1989), however their value is derived from emission-line photometry with appreciable contamination from [N II] λ6583 Å in their measurement of the Hα flux. Hence, we conclude that our measurement (derived using entirely non-blended spectral lines) is a more reliable determination. Furthermore, the galactic latitude of Hen 2-11 (+0.9 degrees) means that high extinction is entirely consistent with purely foreground reddening, although some component may be internal to the object as well.

The nebular spectrum taken with the higher resolution PG 1300 grating was used to measure the heliocentric radial velocity of the nebula, which we determine to be 22.1 ± 2.6 km s^{-1} with the EMSAO program (Kurtz & Mink 1998).

3.3.1. Plasma diagnostics

Using the NEAT code (for full details of the analytic processes and atomic data employed, see Wesson et al. 2012), we measure an electron density of 570 ± 90 cm^{-3} from the [SII] lines, and 1800 ± 1600 cm^{-3} from the [Ar IV] λ4711/4740 Å lines. Although the uncertainty on the [Ar IV] density is large, the discrepancy between these two values may be due to the presence of high density clumps (Zhang et al. 2004); the critical densities of the [S II] lines are 3.625×10^3 and 1.419×10^3 cm^{-3}, while those of the [Ar IV] lines are 1.012×10^5 and 1.630×10^4 cm^{-3}, and so any material at densities of 1×10^5 cm^{-3} would emit [Ar IV] but not [S II].

The temperatures derived from [O III] and [N II] are in excellent agreement at 11500 ± 250 K and 11850 ± 450 K, respectively. The [S III] λ9069/6312 Å line ratio implies a very high temperature, but the λ9069 Å line lies in a vignetted region of the spectrum and its flux is probably underestimated. A factor of 2 increase in its measured flux would bring the [S III] temperature into line with the other diagnostics.

Using the "crossover" method of Kaler & Jacoby (1989), we were able to estimate the central star temperature, given the measured He II/Hβ dereddened flux ratio, to be ~108 000 K – in reasonable agreement with the temperature derived by modelling the lightcurve[5], 140 000 ± 30 000 K.

3.3.2. Empirical analysis

We first carry out an empirical analysis using the NEAT code (Wesson et al. 2012), which propagates the observational uncertainties into the final quantities using a monte carlo technique. Ionic abundances were derived using a temperature of 11 800 K and a density of 500 cm^{-3} for singly ionised species, and 11 500 K and 1800 cm^{-3} for more highly ionised species. Our spectra do not extend as far bluewards as the O II lines at λ3727/3729 Å, and the lines at λ7320/7330 Å lie in a gap in our spectral coverage. Without an O^+/O^{2+} ratio, we are unable to estimate the necessary ionisation correction factors to derive total elemental abundances for any heavy elements. However, the presence of He^{2+} (while still only comprising a relatively small amount of the total He[6]) implies that O^{2+} will be the dominant ionisation stage of oxygen. The absence of O^+ lines introduces a relatively small uncertainty into the O/H abundance, which we find to be $(3.3 \pm 0.3) \times 10^{-4}$, as O^+/O^{2+} will be low. The N/H abundance, on the other hand, is essentially unconstrained as only N^+ is observable; the fraction of N^+ is very small and is impossible to estimate from the current data. We find He/H to be 0.104 ± 0.007; this indicates that Hen 2-11 is not a Type I PN (Peimbert 1978). Table 3 gives the measured and de-reddened line intensities, as well as the ionic abundances calculated using the NEAT code (Wesson et al. 2012), derived from the nebular spectra shown in Fig. 5.

[5] Unlike the Zanstra method, this technique does not depend on the magnitude of the central star, the measurement of which can be heavily skewed for binary systems where a significant proportion of the optical flux originates from the secondary. Even for Hen 2-11, where the primary is intrinsically much brighter than the secondary, the contribution from the secondary is significant at most phases due to the strength of the irradiation effect. This, along with the nebula's optical depth, may account for the discrepancy between our temperature and the hydrogen Zanstra temperature of 89 000 ± 11 000 K (Shaw & Kaler 1989).

[6] A greater fraction of He in He^{2+} would imply that O^{3+} would be the dominant ionisation stage.

3.3.3. Photoionisation modelling

Given that we are unable to estimate the ionisation correction factors needed to empirically derive heavy element abundances, we constructed a photoionisation model using MOCASSIN (Ercolano et al. 2003) to try constrain the N abundance (and further confirm the non-Type I nature of Hen 2-11).

From the images of the nebula (Fig. 1) it is clear that the nebula is irregular and filamentary. However, our long slit spectrum does not provide sufficient observational constraints to realistically model the nebular morphology, nor do we have any information about the surface abundances of the central star which would allow us to realistically estimate the ionising spectrum. Our model is, therefore, highly simplified and is intended only as a first approximation, a more rigorous modelling would require spatially resolved spectroscopy of the nebula.

We modelled the nebula as a sphere with a radius of 10^{18} cm, estimated from our images and the distance of 700 pc derived in Sect. 3.2. Our model had a uniform hydrogen density, with the central star approximated by a blackbody. We then varied the nebular abundances and the central star temperature to achieve a good match to our observed line fluxes.

Our best fitting model has a stellar luminosity of 5140 $L_\odot$ and a temperature of 115 000 K, in good agreement with the values derived in Sect. 3.3.1 although slightly lower than the temperature derived from the light curve modelling (but still within the uncertainty). The emission line fluxes predicted by the model are given alongside the observed values in Table 3.

The model reproduces most line intensities well, in particular the strengths of He I and He II, and the O III nebular to auroral line ratio. The observed [N II] temperature diagnostic ratio is lower than that predicted by the model, indicating that the actual N^+ temperature is higher, and the N^+ abundance even lower than predicted by the model. This may indicate the presence of high-temperature low-ionisation regions of the nebula which are not captured by our simple model (see Sect. 4 for further discussion).

The total abundances used in our model are given in Table 4. These strengthen the indication from the empirical analysis that Hen 2-11 does not have Type I abundances. In particular, the nitrogen abundance in the model is very low, with N/O ~ 0.05; Galactic Type I PNe have N/O > 0.8 (Kingsburgh & Barlow 1994). While this cannot be considered a rigorous determination of the true total abundances, and therefore the true N/O ratio, it does provide a strong indication that the true N/O value will be much lower than for a typical Type I PN.

4. Discussion

The central star of Hen 2-11 has been shown to be a photometric variable with a period of 0.61 d. Modelling of the lightcurve indicates that the system is a post-CE binary with a hot primary, also the nebular progenitor, of temperature of 110–140 kK, and a K-type main sequence secondary of temperature ≈4500 K. These values, as well as the other modelled stellar parameters (size/luminosity), are roughly consistent with evolutionary models and the distances published in the literature.

It is important to point out that given the lack of radial velocity measurements, we can place only very loose constraints on the mass ratio and therefore on the mass of the primary (particularly knowing that the spectral type of the secondary, determined from its modelled temperature, is often at odds with the measured mass in these systems; see below for further discussion) However, our model's best-fitting value of 0.67 $M_\odot$ is a fairly typical remnant mass and fits well with a similarly typical PN

Table 3. Observed, $F(\lambda)$, and dereddened $I(\lambda)$, nebular emission line fluxes relative to Hβ = 100, and the fractional ionic abundance in that line relative to that of hydrogen, $\frac{X(\text{line})}{H}$.

λ	Ion	$F(\lambda)$		$I(\lambda)$		$\frac{X(\text{line})}{H}$		$I_{\text{model}}(\lambda)$
3967.46+3970.07[a]	[Ne III]+H I	14.63	±1.07	47.10	±3.46	-	-	Ne=29.99 H=15.98
4340.47	H I	23.64	±0.40	47.77	±0.92	–	–	47.00
4363.21	[O III]	7.09	±0.40	13.91	±0.82	4.23×10^{-4}	$^{+8.89\times10^{-5}}_{-1.13\times10^{-4}}$	14.08
4471.50	He I	3.00	±0.39	5.09	±0.66	0.098	±0.012	5.41
4685.68	He II	14.32	±4.76	13.25	$^{+2.90}_{-3.72}$	0.011	$^{+2.42\times10^{-3}}_{-3.11\times10^{-3}}$	14.24
4711.37	[Ar IV]	4.25	±0.22	5.23	±0.27	1.07×10^{-6}	$^{+1.87\times10^{-7}}_{-1.92\times10^{-7}}$	5.19
4740.17	[Ar IV]	4.37	±0.86	4.87	$^{+0.83}_{-1.00}$	1.07×10^{-6}	$\pm 2.03 \times 10^{-7}$	4.30
4861.33	H I	100.00	±0.70	100.01	±0.00	–	–	100.00
4958.91	[O III]	541.81	±4.87	474.40	±5.30	3.51×10^{-4}	$\pm 4.91 \times 10^{-5}$	472.30
5006.84	[O III]	1696.82	±4.82	1391.98	±9.67	3.46×10^{-4}	$\pm 4.82 \times 10^{-5}$	1409.35
5412.73	He II	3.24	±0.44	1.54	±0.21	0.013	±0.002	1.31
5754.60	[N II]	5.99	±0.45	2.04	±0.15	1.06×10^{-5}	$^{+9.79\times10^{-7}}_{-1.07\times10^{-6}}$	1.78
5875.66	He I	48.16	±0.46	14.64	±0.16	0.094	$^{+7.59\times10^{-3}}_{-4.87\times10^{-3}}$	14.82
6300.30	[O I]	18.31	±10.94	1.68	$^{+0.59}_{-0.91}$	1.84×10^{-6}	$^{+6.66\times10^{-7}}_{-1.04\times10^{-6}}$	0.76
6312.10	[S III]	12.47	±11.64	0.58	$^{+0.27}_{-0.50}$	6.65×10^{-7}	$^{+6.65\times10^{-7}}_{-3.57\times10^{-7}}$	0.32
6363.77	[O I]	7.43	±10.59	0.07	$^{+0.07}_{-0.14}$	2.39×10^{-7}	$^{+2.39\times10^{-7}}_{-4.73\times10^{-7}}$	0.38
6548.10	[N II]	197.20	±12.59	33.77	±2.16	1.16×10^{-5}	$\pm 1.38 \times 10^{-6}$	36.44
6562.77	H I	1680.91	±11.84	284.62	$^{+0.87}_{-0.71}$	–	–	283.83
6583.50	[N II]	549.71	±11.99	91.53	±2.13	1.03×10^{-5}	$\pm 9.80 \times 10^{-7}$	111.30
6678.16	He I	25.82	±10.08	2.60	$^{+0.65}_{-0.86}$	0.067	$^{+0.016}_{-0.022}$	4.14
6716.44	[S II]	88.57	±2.06	13.30	±0.33	4.29×10^{-7}	$\pm 3.62 \times 10^{-8}$	13.16
6730.82	[S II]	85.22	±2.07	12.66	±0.33	4.30×10^{-7}	$\pm 3.63 \times 10^{-8}$	12.64
7065.25	He I	21.84	±2.10	2.54	±0.25	0.102	±0.010	2.96
7135.80	[Ar III]	151.84	±2.02	16.84	±0.28	1.21×10^{-6}	$\pm 1.23 \times 10^{-7}$	12.59
7281.35	He I	6.09	±5.95	0.13	$^{+0.06}_{-0.11}$	0.02	$^{+8.09\times10^{-3}}_{-0.02}$	0.84
7751.43	[Ar III]	52.08	±2.98	3.91	±0.23	1.17×10^{-6}	$\pm 1.37 \times 10^{-7}$	3.02
9068.60	[S III]	352.73	±4.24	13.75	±0.26	1.42×10^{-6}	$\pm 1.25 \times 10^{-7}$	8.04
4740/4711	[Ar IV]	–	–	0.93	$^{+0.20}_{-0.16}$	–	–	0.83
6731/6717	[S II]	–	–	0.95	±0.03	–	–	0.96
(4959+5007)/4363	[O III]	–	–	134.05	±7.96	–	–	133.60
(6584+6548)/5754	[N II]	–	–	61.94	±4.92	–	–	82.92

Notes. The final column shows the fluxes predicted by our MOCASSIN photoionisation model. The lower part of the table lists a series of emission line diagnostic ratios and their measured and modelled values. [(a)] The value measured in the spectrum is a blend of the two lines listed, while the model values are for the individual components

age (even accounting for the fairly large uncertainty in the relatively arbitrary starting time of the evolutionary tracks). Without further observations we cannot place any stronger constraints on the system parameters, other than to say that all aspects of the model are consistent with current observations and those of similar systems.

For the modelled system, we would expect to observe radial velocity variations of around 40 km s^{-1} ($K_2 \approx 20$ km s^{-1} about our measured nebular heliocentric velocity of ≈21 km s^{-1}). We, therefore, strongly encourage further spectroscopic follow-up of the system in the form of a time-resolved radial velocity study. Given the extremely large reflection effect in the system, one would expect the secondary to show very strong C III and N III emission lines at almost all phases (Corradi et al. 2011; Miszalski et al. 2011b), thus making Hen 2-11 particularly apt for radial velocity study in spite of its intrinsic faintness. Unfortunately, our two spectra covering these lines were taken very close to primary eclipse such that the irradiated face of the secondary was not observed, and therefore these lines were not detected. However, such a radial velocity study would allow the determination of key system parameters such as the mass ratio and individual component masses. The component masses

Table 4. Abundances used in the photoionisation model of Hen 2-11.

Element	Abundance
H	1.0
He	0.104
C	0.8×10^{-4}
N	3.0×10^{-5}
O	5.5×10^{-4}
Ne	7.5×10^{-5}
S	1.1×10^{-6}
Ar	1.8×10^{-6}

are essential, not only to test the model, but also to compare the binary parameters to those of other post-CE central stars. In general, the secondaries, in the few systems that have been the subject of detailed study, are found to display inflated radii and increased spectral temperatures with respect to those expected from their masses (Pollacco & Bell 1993; De Marco et al. 2008; Afşar & Ibanoğlu 2008). As such, it would be of great interest to add further statistics in this small sample. If this were the case for Hen 2-11, the secondary mass might be expected to be more like that of a late K- or early M-type main sequence star (reducing the primary mass to possibly be more in line with that of Abell 46, another eclipsing post-CE central star displaying a large reflection effect, assuming a similar mass ratio to that determined by the lightcurve modelling; Pollacco & Bell 1994).

Little data exists on the nebular abundances of post-CE PNe, unfortunately our data do not permit us to perform a full analysis and derive total elemental abundances. We have derived ionic abundances where possible, and shown that Hen 2-11 is not a Peimbert Type I nebula. This could be taken as an indication of the common-envelope cutting short the AGB evolution of the nebular progenitor, but this is difficult to assess without accurate C/O and N/O ratios (De Marco 2009). We, therefore, constructed a photoionisation model of the nebula to provide an estimate of these ratios and test the validity of this scenario. Unfortunately, as clearly shown by the imagery in Fig. 1, the nebula is far from homogenous and this is borne out in the results of our modelling. These inhomogeneities are present throughout the nebula not only in density but also in temperature and chemistry, meaning that the derived estimates for C/O and N/O in the nebula are highly uncertain (N/O particularly so, given the discrepancy between observed and modelled temperature) meaning that the true values may indeed be greater. However, in spite of this uncertainty, it remains clear that the nebula is both carbon and nitrogen poor, consistent with a binary partner cutting short the AGB evolution of the nebular progenitor.

The recent spate of discoveries, of short period CSPNe with main sequence secondaries (this work; Miszalski et al. 2011b; Corradi et al. 2011), further highlights the discrepancy between the observed post-CE period distribution and that predicted by population synthesis models (even when accounting for observational biases, De Marco et al. 2008; Rebassa-Mansergas et al. 2008; Miszalski et al. 2009a). Knowledge of all system parameters (only possible through radial velocity study) is key in further constraining the downfalls of these population synthesis models.

Morphologically, Hen 2-11 appears remarkably similar to two other PNe proven to host post-CE central stars, NGC 6326 and NGC 6778. However, in spite of the fact that their central binaries have shorter periods (0.372 and 0.1534 d, respectively), that of Hen 2-11 shows a much more pronounced reflection effect. The strength of this effect depends on several factors including inclination, temperature and mass ratio. In the case of NGC 6778 (the shortest period of the three), inclination would not seem to be an adequate explanation given its eclipsing nature and the measured inclination of the nebula (~78°; Guerrero & Miranda 2012). Therefore the difference in amplitude could be attributed to a combination of NGC 6778 hosting a colder white dwarf and a difference in mass ratio between the two systems. The difference in mass ratio is difficult to assess without detailed modelling of the central binary of NGC 6778 (however it is estimated to be around 0.5; Guerrero & Miranda 2012), but a colder central star is clearly feasible given that Hen 2-11 is roughly at the hottest point of its evolution (Fig. 3) and the age difference between the systems implies NGC 6778 should be yet to reach that point (around 2000 years cf. 7000 years for Hen 2-11; Guerrero & Miranda 2012). This hypothesis is further supported by the temperatures of the central stars, where that of Hen 2-11 is found to be ~108 000 K (using our measured He II/Hβ dereddened flux ratio and the relation of Kaler & Jacoby 1989, and in reasonable agreement with the primary temperature in our best fitting lightcurve model) cf. ~50 000 K for NGC 6778 (derived using a similar methodology, known as the energy balance method, by Preite-Martinez & Pottasch 1983).

In addition to detailed study of their central stars, it is important that these objects are subjected to detailed spatio-kinematical study, in order to ascertain the three-dimensional morphology and velocity structure of the nebula, which can then be related to the evolution and parameters of the central star system (particularly the inclination of nebular symmetry axis with respect to that of the binary orbital plane; Jones et al. 2011, 2012; Tyndall et al. 2012). To that end, we strongly encourage the acquisition of high-resolution, spatially-resolved spectroscopy (either longslit or integral field) of the nebulae Hen 2-11 and NGC 6326 (NGC 6778 has already been the subject of detailed study; Guerrero & Miranda 2012). This data would also indicate whether the structures in the northwest and southeastern parts of the nebula are akin to the jets/outflows seen in other binary PNe, and if so whether they were formed contemporaneously to the central region or before – a strong indication of a phase of pre-CE mass transfer (Boffin et al. 2012b; Corradi et al. 2011; Miszalski et al. 2013a).

Finally, it is worthwhile to note that Hen 2-11 has been observed with the *Chandra* X-ray Observatory as part of the *Chandra* Planetary Nebulae Survey (ChanPlaNS; Kastner et al. 2012), and, as such, represents an important test case of a close binary central star in the local sample.

Acknowledgements. We thank the anonymous referee for their comments which helped to improve the clarity of the manuscript. Based on observations made with ESO Telescopes at the La Silla Paranal Observatory under programme IDs 088.D-0573 and 090.D-0693, and the Southern African Large Telescope (SALT) under programme 2012-2-RSA-002. This work was co-funded under the Marie Curie Actions of the European Commission (FP7-COFUND). This research has made use of NASA's Astrophysics Data System Bibliographic Services. This research has made use of the SIMBAD database, operated at the CDS, Strasbourg, France.

References

Acker, A., Marcout, J., Ochsenbein, F., et al. 1992, The Strasbourg-ESO Catalogue of Galactic Planetary Nebulae. Parts I, II (European Southern Observatory)
Afşar, M., & Ibanoğlu, C. 2008, MNRAS, 391, 802
Bertin, E., & Arnouts, S. 1996, A&AS, 117, 393
Boffin, H. M. J., Miszalski, B., & Jones, D. 2012a, A&A, 545, A146
Boffin, H. M. J., Miszalski, B., Rauch, T., et al. 2012b, Science, 338, 773
Boyajian, T. S., von Braun, K., van Belle, G., et al. 2012, ApJ, 757, 112
Buckley, D. A. H., Burgh, E. B., Cottrell, P. L., et al. 2006, in Proc. SPIE, 6269, 0A
Burgh, E. B., Nordsieck, K. H., Kobulnicky, H. A., et al. 2003, in Proc. SPIE 4841, eds. M. Iye, & A. F. M. Moorwood, 1463

Buzzoni, B., Delabre, B., Dekker, H., et al. 1984, The Messenger, 38, 9
Ciardullo, R., Bond, H. E., Sipior, M. S., et al. 1999, AJ, 118, 488
Corradi, R. L. M., Sabin, L., Miszalski, B., et al. 2011, MNRAS, 410, 1349
Crawford, S. M., Still, M., Schellart, P., et al. 2010, in Proc. SPIE, 7737, 25
De Marco, O. 2009, PASP, 121, 316
De Marco, O., Hillwig, T. C., & Smith, A. J. 2008, AJ, 136, 323
Dhillon, V. S., Privett, G. J., & Duffey, K. P. 2001, Starlink User Note 167.6 (Rutherford Appleton Laboratory)
Ducati, J. R., Bevilacqua, C. M., Rembold, S. B., & Ribeiro, D. 2001, ApJ, 558, 309
Epchtein, N., Deul, E., Derriere, S., et al. 1999, A&A, 349, 236
Ercolano, B., Barlow, M. J., Storey, P. J., & Liu, X.-W. 2003, MNRAS, 340, 1136
Górny, S. K., Schwarz, H. E., Corradi, R. L. M., & Van Winckel, H. 1999, A&AS, 136, 145
Guerrero, M. A., & Miranda, L. F. 2012, A&A, 539, A47
Gutiérrez-Moreno, A., Anguita, C., Loyola, P., & Moreno, H. 1999, PASP, 111, 1163
Henize, K. G. 1967, ApJS, 14, 125
Howarth, I. D. 1983, MNRAS, 203, 301
Jones, D. 2011, Ph.D. thesis, Jodrell Bank Centre for Astrophysics, University of Manchester, UK
Jones, D., Lloyd, M., Santander-García, M., et al. 2010, MNRAS, 408, 2312
Jones, D., Tyndall, A. A., Huckvale, L., Prouse, B., & Lloyd, M. 2011, in Evolution of Compact Binaries, eds. L. Schmidtobreick, M. R. Schreiber, & C. Tappert, ASP Conf. Ser., 447, 165
Jones, D., Mitchell, D. L., Lloyd, M., et al. 2012, MNRAS, 420, 2261
Kaler, J. B. 1989, Stars and their spectra. An introduction to spectral sequence (Cambridge University Press)
Kaler, J. B., & Jacoby, G. H. 1989, ApJ, 345, 871
Kastner, J. H., Montez, Jr., R., Balick, B., et al. 2012, AJ, 144, 58
Kingsburgh, R. L., & Barlow, M. J. 1994, MNRAS, 271, 257
Kobulnicky, H. A., Nordsieck, K. H., Burgh, E. B., et al. 2003, in Proc. SPIE 4841, eds. M. Iye, & A. F. M. Moorwood, 1634
Kurtz, M. J., & Mink, D. J. 1998, PASP, 110, 934
Kurucz, R. L. 1993, VizieR Online Data Catalog: VI/39
Miszalski, B., Acker, A., Moffat, A. F. J., Parker, Q. A., & Udalski, A. 2008, A&A, 488, L79
Miszalski, B., Acker, A., Moffat, A. F. J., Parker, Q. A., & Udalski, A. 2009a, A&A, 496, 813
Miszalski, B., Acker, A., Parker, Q. A., & Moffat, A. F. J. 2009b, A&A, 505, 249
Miszalski, B., Corradi, R. L. M., Boffin, H. M. J., et al. 2011a, MNRAS, 413, 1264
Miszalski, B., Jones, D., Rodríguez-Gil, P., et al. 2011b, A&A, 531, A158
Miszalski, B., Boffin, H. M. J., & Corradi, R. L. M. 2013a, MNRAS, 428, L39
Miszalski, B., Boffin, H. M. J., Jones, D., et al. 2013b, MNRAS, 436, 3068
O'Donoghue, D., Buckley, D. A. H., Balona, L. A., et al. 2006, MNRAS, 372, 151
Peimbert, M. 1978, in Planetary Nebulae, ed. Y. Terzian, IAU Symp., 76, 215
Pollacco, D., & Bell, S. A. 1993, MNRAS, 262, 377
Pollacco, D., & Bell, S. A. 1994, MNRAS, 267, 452
Preite-Martinez, A., & Pottasch, S. R. 1983, A&A, 126, 31
Rebassa-Mansergas, A., Gänsicke, B. T., Schreiber, M. R., et al. 2008, MNRAS, 390, 1635
Shaw, R. A., & Kaler, J. B. 1989, ApJS, 69, 495
Snodgrass, C., Saviane, I., Monaco, L., & Sinclaire, P. 2008, The Messenger, 132, 18
Stanghellini, L., Shaw, R. A., & Villaver, E. 2008, ApJ, 689, 194
Tocknell, J., De Marco, O., & Wardle, M. 2013 [arXiv:1308.5027]
Tyndall, A. A., Jones, D., Lloyd, M., O'Brien, T. J., & Pollacco, D. 2012, MNRAS, 422, 1804
Tyndall, A. A., Jones, D., Boffin, H. M. J., et al. 2013, MNRAS, 436, 2082
van Dokkum, P. G. 2001, PASP, 113, 1420
Vassiliadis, E., & Wood, P. R. 1994, ApJS, 92, 125
Wesson, R., Stock, D. J., & Scicluna, P. 2012, MNRAS, 422, 3516
Zhang, Y., Liu, X.-W., Wesson, R., et al. 2004, MNRAS, 351, 935